1521-009X/12/4012-2221–2230$25.00
DRUG METABOLISM AND DISPOSITION
Vol. 40, No. 12
48298/3803696
DMD 40:2221–2230, 2012

Cytochrome P450 3A5 Plays a Prominent Role in the Oxidative Metabolism of the Anti-Human Immunodeficiency Virus Drug Maraviroc[S]

Yanhui Lu, Craig W. Hendrix, and Namandjé N. Bumpus

Department of Pharmacology and Molecular Sciences (Y.L., C.W.H., N.N.B.), and Division of Clinical Pharmacology, Department of Medicine (C.W.H.), The Johns Hopkins University School of Medicine, Baltimore, Maryland

Received July 30, 2012; accepted August 24, 2012

ABSTRACT:

Maraviroc is an anti-human immunodeficiency virus drug that acts by blocking viral entry into target cells. With use of ultra-performance liquid chromatography-mass spectrometry several monooxygenated, dioxygenated, and glucuronidated metabolites of maraviroc were identified both in vitro and in vivo. Characterization of the enzymes involved in the production of these metabolites determined that cytochrome P450 3A5 was the principal enzyme responsible for the formation of an abundant metabolite of maraviroc that resulted from oxygenation of the dichlorocyclohexane ring. For the formation of this metabolite, the V_{max} values for CYP3A4 and CYP3A5 were 0.04 and 0.93 pmol · min^{-1} · pmol P450^{-1}, and the K_m values were 11.1 and 48.9 μM, respectively. Furthermore, human liver microsomes isolated from donors homozygous for the loss-of-function *CYP3A5*3* allele exhibited a 79% decrease in formation of this metabolite compared with those homozygous for the wild-type *CYP3A5*1* allele. To probe which divergent residues between CYP3A4 and CYP3A5 might play a role in the differential activities of these enzymes toward maraviroc, mutations were introduced into both enzymes and metabolism of maraviroc was measured. A CYP3A5 L57F mutant exhibited a 61% decrease in the formation of this metabolite, whereas formation by a CYP3A4 F57L mutant was increased by 337% compared with that of the wild type. Taken together, these data provide novel insights into the biotransformation of maraviroc as well as the potential role of CYP3A4 and CYP3A5 divergent residues in the enzymatic activities of these two highly homologous enzymes.

Introduction

Maraviroc is an anti-HIV drug that acts by blocking the virus coreceptor, chemokine receptor CCR5, at the viral entry step, thereby preventing viral infection (Dorr et al., 2005; Fätkenheuer et al., 2005). In addition, there is increased interest in the development of maraviroc as an oral and/or topical microbicide for use in HIV prevention. Although maraviroc is known to be extensively metabolized to a number of products (Abel et al., 2008a), a comprehensive analysis of the biotransformation of maraviroc has yet to be reported. The cytochromes P450 (P450) are a superfamily of heme-containing monooxygenases that play a crucial role in drug clearance. The CYP3A subfamily enzymes, CYP3A4 and CYP3A5, are responsible for the metabolism of more than 50% of drugs currently on the market (Rendic and Di Carlo, 1997). They share 84% amino acid sequence identity and 92% similarity, resulting in overlapping substrate specificities (Pearson et al., 2007). Therefore, defining their respective contributions to drug metabolism as well as drug-drug interactions remains challenging. It is well established that CYP3A5 is polymorphically expressed, with the wild-type *CYP3A5*1* allele being associated with the highest level of protein expression, whereas variant alleles such as *CYP3A5*3* lead to decreased expression or no activity due to alternative mRNA splicing (Hustert et al., 2001; Kuehl et al., 2001). In individuals that carry at least one *CYP3A5*1* allele, CYP3A5 protein accounts for at least 50% of the total hepatic CYP3A content (Kuehl et al., 2001). The expression of CYP3A5 is highly variable among different ethnic populations. For instance, the *CYP3A5*3* allele is abundantly present in the European American population with a frequency of 85 to 98%, whereas it is much less common in the African American population with a frequency of 27 to 48% (Hustert et al., 2001; Kuehl et al., 2001; van Schaik et al., 2002; Daly, 2006). In addition, increased risk of certain drug toxicities has been reported in people who have low expression of CYP3A5 (Egbelakin et al., 2011; Hooper et al., 2012; Takashina et al., 2012).

To date, several CYP3A4 crystal structures have been solved, whereas the structure of CYP3A5 is not yet available. Six CYP3A4 substrate recognition sites (SRS1–6) were identified and experimentally demonstrated to be important for substrate binding and catalytic activity (Harlow and Halpert, 1997; He et al., 1997; Domanski et al., 1998; Wang et al., 1998; Khan and Halpert, 2000; Roussel et al.,

This work was supported by the Pharmaceutical Research and Manufacturers of America Foundation; National Institutes of Health HIV Prevention Trials Network [Grant 5UM1-AI068613]; National Institutes of Health National Center for Research Resources [Grant 1S10-RR027733]; and Pendleton Foundation Trust.

Article, publication date, and citation information can be found at http://dmd.aspetjournals.org.

http://dx.doi.org/10.1124/dmd.112.048298.

[S] The online version of this article (available at http://dmd.aspetjournals.org) contains supplemental material.

ABBREVIATIONS: HIV, human immunodeficiency virus; P450, cytochrome P450; SRS, substrate recognition site; UGT, UDP-glucuronosyltransferase; UPLC, ultra-performance liquid chromatography; MS, mass spectrometry.

2000; Khan et al., 2002). Phenylalanine residues Phe108, Phe213, Phe215, Phe219, Phe220, Phe241, and Phe304 form a hydrophobic roof of the CYP3A4 active site above the heme between SRS1, SRS2, SRS3, and SRS4 (Williams et al., 2004; Yano et al., 2004). Another phenylalanine residue, Phe57, falls into a region recently denoted as SRS1′a (Zawaira et al., 2011) and is important for CYP3A4 substrate binding (Sevrioukova and Poulos, 2010). In contrast, information regarding the importance of particular CYP3A5 active site residues is very limited. Because of the high similarity between CYP3A4 and CYP3A5, the overall folding of CYP3A5 has been predicted to be largely similar to that of CYP3A4 (Pearson et al., 2007). Mutation of divergent SRS residues of CYP3A4 to the corresponding amino acids of CYP3A5, P107S, F108L, N206S, L210F, V376T, S478D, and L479T resulted in a shift of the aflatoxin B1 metabolite profile of CYP3A4 toward that of CYP3A5 (Wang et al., 1998). However, the effects of the reverse mutations on CYP3A5 activity remain unknown.

In the present study, we report the enzymes involved in maraviroc oxidative metabolism. Our enzyme kinetic studies revealed that CYP3A5 has a higher capacity to metabolize maraviroc to a major monooxygenated metabolite than CYP3A4. Plasma and urine isolated from a human subject genotyped as wild-type for CYP3A5 confirmed that this metabolite is, indeed, the most abundant maraviroc product formed in vivo. Furthermore, we then leveraged this observation and systematically mutated CYP3A5 toward CYP3A4 using formation of this metabolite as an activity probe to identify residues in CYP3A5 that confer specificity with regard to maraviroc metabolism. In addition, we identified four novel dioxygenated maraviroc metabolites and two glucuronidated metabolites and confirmed their existence in human urine samples. Taken together, these studies provide novel mechanistic insight into the phase I and phase II metabolism of maraviroc as well as the role of divergent amino acids of CYP3A4 and CYP3A5 in influencing the catalytic activities of these two highly homologous enzymes.

Materials and Methods

Materials. Maraviroc was obtained from the National Institutes of Health AIDS Research and Reference Reagent Program (Germantown, MD). Maraviroc-d_6, 3-hydroxymethyl maraviroc, and 4-hydroxyphenyl maraviroc were obtained from Toronto Research Chemicals, Inc. (North York, ON, Canada). Quinidine, ketoconazole, sulfaphenazole, (+)-*N*-3-benzylnirvanol, and furafylline were purchased from Sigma-Aldrich (St. Louis, MO). 2-Phenyl-2-(1-piperidinyl) propane was bought from Santa Cruz Biotechnology, Inc. (Santa Cruz, CA). Pooled human liver microsomes (20 mg/ml, pool of 200, mixed gender) and one lot of *CYP3A5**3/*3 human liver microsomes were purchased from XenoTech, LLC (Lenexa, KS). The NADPH-regenerating system, UGT Reaction Mix [consisting of two reagents: solution A (25 mM UDP-glucuronic acid) and solution B (5× UGT assay buffer containing alamethicin)], CYP3A4 and CYP3A5 primary antibodies, *CYP3A5**1/*1 and *CYP3A5**3/*3 human liver microsomes, and Supersomes containing cDNA-expressed human CYP1A2, CYP2B6, CYP2C8, CYP2C9*1, CYP2C19, CYP2D6*1, CYP3A4, and CYP3A5, coexpressed with reductase, were purchased from BD Biosciences (San Jose, CA). The β-actin antibody and cell lysis buffer were obtained from Cell Signaling Technology (Danvers, MA). The bicinchoninic acid assay kit and SuperSignal West Dura Chemiluminescent Substrate were obtained from Thermo Fisher Scientific (Waltham, MA).

Incubation Conditions for Human Liver Microsome Metabolism Experiments. The metabolism experiments using human liver microsomes were performed in a volume of 500 μl in 10 × 75 mm borosilicate glass tubes (Thermo Fisher Scientific). One microliter of 10 mM maraviroc in methanol was added into a 500-μl reaction system containing 0.1 M potassium phosphate buffer (pH 7.4) and 0.5 mg/ml human liver microsomes and incubated for 5 min at 37°C in a water bath. The reaction was initiated by addition of the NADPH-regenerating system and allowed to proceed for 30 min at 37°C. For the chemical inhibition assays, furafylline (20 μM), 2-phenyl-2-(1-piperidinyl) propane (30 μM), sulfaphenazole (20 μM), (+)-*N*-3-benzylnirvanol (10 μM), quinidine (10 μM), and ketoconazole (10 μM) were used to inhibit CYP1A2, CYP2B6, CYP2C9, CYP2C19, CYP2D6, and CYP3A4/5, respectively, to investigate the involvement of these individual P450 enzymes in the formation of maraviroc oxidative metabolites. The inhibitors were preincubated with the human liver microsomes and NADPH-regenerating system for 10 min before the addition of 1 μl of 10 mM maraviroc to initiate the reactions. For reactions containing *CYP3A5* genotyped human liver microsomes, a final concentration of 2 μM maraviroc was used in a total reaction volume of 250 μl with other components being kept at the same concentrations as described above. For glucuronidation reactions, UGT reaction solutions containing 25 mM UDP-glucuronic acid and 5× UGT assay buffer with alamethicin were added into the above pooled human liver microsome reaction systems after addition of the NADPH-regenerating system.

Incubation Conditions for Individual cDNA-Expressed P450s. One picomole of human recombinant P450 enzyme (CYP1A2, CYP2B6, CYP2C8, CYP2C9*1, CYP2C19, CYP2D6*1, CYP3A4, or CYP3A5) was preincubated with 20 μM maraviroc in 0.1 M potassium phosphate buffer (pH 7.4) at 37°C for 5 min, and the reaction was initiated by addition of the NADPH-regenerating system (final reaction volume of 100 μl) and continued for 30 min at 37°C.

Enzyme Kinetics for CYP3A4 and CYP3A5. Maraviroc stock solution (600 mM) was prepared in dimethyl sulfoxide and diluted into working solutions (0.02, 0.2, 2, 6, 20, 60, and 200 mM). The working solution (0.5 μl of each) was then preincubated with 13 pmol of CYP3A4 or CYP3A5 at 37°C for 5 min in 0.1 M potassium phosphate buffer (pH 7.4). The final concentrations of maraviroc were 0.1, 1, 10, 30, 100, 300, and 1000 μM in a total reaction volume of 100 μl. The reaction was initiated by addition of the NADPH-regenerating system and allowed to proceed for 30 min at 37°C.

The enzyme concentrations as well as the incubation time were chosen on the basis of preliminary results demonstrating that the formation of oxidative metabolites was linear under these conditions. The metabolite concentrations were estimated against a standard curve with a range of 0.024 to 200 pmol of maraviroc.

Sample Preparation after Incubation. At the end of the incubation, 2 reaction volumes of acetonitrile were added to stop the reaction. The internal standard maraviroc-d_6 (100 μl of 20 ng/ml), an analog of maraviroc labeled with 6 deuteriums, was added, and the samples were vortexed. The mixture was then centrifuged at 3000*g* for 10 min at 4°C, and the supernatants were dried under a stream of nitrogen gas at 50°C. The samples were reconstituted in 50 μl of methanol and transferred to vials containing 40 μl of 5% acetonitrile-95% water-0.1% formic acid for injection onto the ultra-performance liquid chromatography (UPLC)-mass spectrometry (MS) system.

Analysis of Maraviroc and Metabolites Using UPLC-MS. Maraviroc and its metabolites were detected by UPLC-MS using an ACQUITY ultra-performance liquid chromatograph (Waters, Milford, MA) interfaced to an AB SCIEX QTRAP 5500 mass spectrometer (Applied Biosystems/MDS Sciex, Foster City, CA). Aliquots of reconstituted samples were injected onto a 1.7-μm UPLC BEH 2.1 × 100 mm C8 column (Waters). Analyte resolution was achieved at a flow rate of 0.35 ml/min with chromatography at room temperature. Mobile phases were 5% acetonitrile-0.1% formic acid in water (A) and 5% water-0.1% formic acid in acetonitrile (B), programmed at 0% B from 0 to 1.1 min, 20% B from 32 to 33 min, and 0% B from 33.1 to 34 min. Detection of the analytes and the internal standard was achieved via multiple reaction monitoring for quantification under positive mode. The monooxygenated maraviroc metabolites were monitored using *m/z* of precursor/product ion pairs at 530/296 and 530/280. The dioxidative metabolites were monitored at *m/z* 546/421, and the glucuronidated metabolites were monitored at *m/z* 706/581 and 706/389. Maraviroc and the internal standard maraviroc-d_6 were monitored at *m/z* of 514/389 and 520/389, respectively. The N-dealkylated metabolite of maraviroc was monitored at *m/z* of precursor/product ion pairs at 235/110. For maraviroc metabolite identification, MS^3 scans were performed with first/second precursor ions of maraviroc, monooxygenated, and dioxygenated metabolites at *m/z* 514/280, 530/296, and 546/312, respectively. For glucuronides, MS^3 scans were performed with first/second precursor ions at *m/z* 706/581 and at *m/z* 706/389. All the data were acquired under positive mode and analyzed by Analyst software (version 1.5.1; Applied Biosystems/MDS Sciex) in Windows XP Professional Version 2002.

Maraviroc Metabolite Analysis in Human Plasma and Urine. A healthy male subject was recruited for maraviroc oxidative metabolite analysis after providing written informed consent for participation in a protocol approved by the institutional review board of Johns Hopkins Medical Institutions. The subject was genotyped for *CYP3A5* using a previously reported method (Kuehl et al., 2001). A single dose of 300 mg of maraviroc was administered orally followed by blood and urine collection over a 24-h period. Blood (10 ml) samples were collected into a heparinized tube predose and 1, 2, 4, 6, 8, and 24 h after administration. Urine samples were collected with intervals of 0 to 2, 2 to 4, 4 to 6, 6 to 8, and 8 to 24 h after drug administration. Plasma was prepared by centrifugation of blood at 1000*g* for 10 min at 4°C. For metabolite analysis, 100 μl of plasma was mixed with 300 μl of methanol. After centrifugation, the supernatant was dried and reconstituted for analysis as described above by UPLC-MS. For urine samples, 100 μl of sample was directly dried and reconstituted using methanol for metabolite analysis.

Site-Directed Mutagenesis and Expression of CYP3A4 and CYP3A5. Plasmids pCMV6-XL4 containing CYP3A4 and CYP3A5 full-length cDNAs (TrueClones) were obtained from OriGene (Rockville, MD). Mutations were made with primers (Supplemental Table 1) using a QuikChange lightning site-directed mutagenesis kit following the manufacturer's instructions. Plasmid DNA was isolated using a GeneJET Plasmid Miniprep Kit (Thermo Fisher Scientific), and DNA sequencing was performed to confirm the presence of a desired mutation and the absence of extraneous mutations. The plasmid constructs (4 μg) were transfected into COS-7 cells using Lipofectamine 2000 (Invitrogen, Carlsbad, CA) according to the manufacturer's instruction.

Analysis of Metabolite Formation by CYP3A4 and CYP3A5 Expressed in COS-7 Cells. Twenty-four hours after transfection, maraviroc was added to a final concentration of 20 μM in 1 ml of Dulbecco's modified Eagle's medium per well. After 40 min of incubation, 600 or 300 μl of medium were transferred to glass tubes and mixed with 50 μl of 20 ng/ml maraviroc-d_6 for cells expressing CYP3A4 and CYP3A5, respectively. Two volumes of acetonitrile were added, vortexed, and centrifuged at 3000*g* for 10 min at 4°C. Supernatants were transferred, dried, reconstituted, and analyzed following the procedure described above.

Immunoblot Analysis of CYP3A4 and CYP3A5 Expression. Cells were harvested in 1 ml of phosphate-buffered saline followed by centrifugation at 500*g* for 5 min at 4°C. The cell pellets were then resuspended in cell lysis buffer containing freshly added phosphatase and protease inhibitor cocktail (Thermo Fisher Scientific Halt Protein and Phosphatase Inhibitor Cocktail) and phenylmethylsulfonyl fluoride. The resuspended cell pellets were passed 30 times through a 25-gauge needle for lysis and centrifuged at 14,000*g* for 10 min at 4°C. Protein concentrations were measured using a bicinchoninic acid assay kit (Thermo Fisher Scientific), and 20 μg of total protein was loaded onto a 10% polyacrylamide gel for separation by SDS-polyacrylamide gel electrophoresis. Immunoblotting was performed using anti-CYP3A4 and anti-CYP3A5 antibodies and β-actin for normalization. A Carestream 4000R system was used for chemiluminescent imaging followed by densitometric analysis.

Statistical Analysis. K_m and V_{max} values were determined by nonlinear regression analysis using GraphPad Prism 5 for Windows (GraphPad Software Inc., San Diego, CA). All data presented are means ± S.D. from three independent experiments performed in duplicate. Two-tailed unpaired *t* tests were performed for comparisons, and $P \leq 0.05$ was considered statistically significant.

Results

Detection of Monooxygenated Metabolites of Maraviroc Using UPLC-MS. With the use of a novel UPLC-MS method that was specifically developed for the detection and separation of all the oxidative metabolites of maraviroc, six major monooxidative metabolites were identified from incubations with human liver microsomes. Herein, these metabolites are denoted as metabolite 1 to metabolite 6 (M1–M6; numbered by order of elution) with retention times of 14.9, 16.2, 16.9, 21.7, 22.6, and 27.0 min, respectively (Fig. 1B). Among the six metabolites, M1, M2, and M3 were the predominant metabolites. To confirm the formation of these monooxygenated products of maraviroc in vivo, a single 300-mg dose of maraviroc was administered orally to a healthy volunteer followed by blood and urine collection and metabolite analysis using UPLC-MS. Genotyping results of *CYP3A5* determined this subject to be homozygous for wild-type *CYP3A5* allele *1. We found that these six metabolites were the major products present in both plasma (Fig. 1C) and urine (Fig. 1D). A secondary amine product resulting from N-dealkylation of maraviroc has been previously found in plasma and excreta (Abel et al., 2008a; Hyland et al., 2008). Therefore, to gain a more comprehensive view of maraviroc biotransformation, we also monitored the formation of this metabolite using our assay. We found that the peak area ratio of formation of this N-dealkylated metabolite to M1 by human liver microsomes was 0.3. In addition, consistent with previous find-

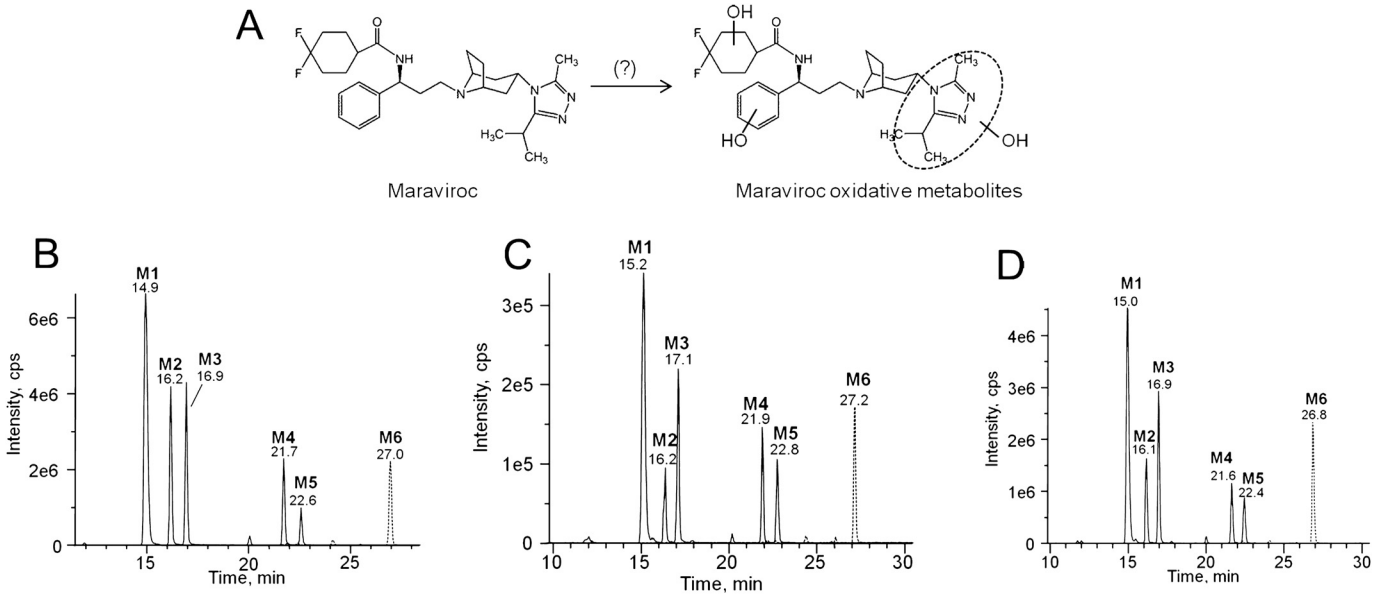

FIG. 1. A novel chromatographic method for the separation of maraviroc oxidative metabolites. A, chemical structure of maraviroc and sites of oxidative metabolism (Abel et al., 2008a). Separation of oxidative metabolites from human liver microsomal reactions (B), human plasma (C), and human urine (D). The human plasma and urine chromatograms are representative of data obtained 2 and 2 to 4 h, respectively, after a single oral dose of 300 mg of maraviroc. Metabolites were analyzed by mass spectrometry using the transitions *m/z* 530 → 296 for M1 to M5 and 530 → 280 for M6 after separation on an UPLC column.

ings, we also detected the N-dealkylated metabolite of maraviroc in both human plasma and urine samples. The peak area ratio of the N-dealkylated maraviroc to M1 ranged from 0.3 to 2.6 and 1.4 to 6.4 in plasma and urine samples, respectively, over a period of 24 h after a single oral dose of maraviroc administration.

CYP3A5 Has a Higher Capacity to Form M1 Than CYP3A4. To determine which P450 isozymes play a role in the formation of these metabolites, maraviroc was incubated with a panel of cDNA-expressed P450s. As shown in Fig. 2A, CYP3A4 and CYP3A5 were essentially the only enzymes that catalyzed the formation of monooxygenated products of maraviroc. Among the six metabolites, M1 was the most abundant and formation by CYP3A5 was 9.7-fold greater than by CYP3A4. To further confirm the role of CYP3A4 and CYP3A5 in M1 formation, maraviroc was incubated with human liver microsomes in the presence of inhibitors of CYP1A2, CYP2B6, CYP2C9, CYP2C19, CYP2D6, and CYP3A4/5 (Fig. 2B). Ketoconazole, an inhibitor of CYP3A4/5, significantly reduced the activity by 81% ($P < 0.001$). Quinidine, a CYP2D6 inhibitor, decreased formation of M1 by 16%; however, this was not statistically significant compared with the vehicle control ($P = 0.12$). The V_{max} values for M1 formation by CYP3A4 and CYP3A5 were 0.04 ± 0.001 and 0.93 ± 0.04 pmol · min^{-1} · pmol P450^{-1}, respectively, and the K_m values were 11.1 ± 2.1 μM and 48.9 ± 7.6 μM, respectively (Fig. 2C). At 1 μM maraviroc, which is within the clinically useful range of maraviroc concentrations, formation by CYP3A5 was 9-fold higher than that of CYP3A4, indicating that CYP3A5 may play a predominant role in the formation of M1 at pharmacologically relevant concentrations of maraviroc.

Reduced M1 Formation by Human Liver Microsomes Genotyped as Homozygous for the Loss-of-Function *CYP3A5*3* Allele. The expression and activity of CYP3A5 has been reported to be affected by genetic polymorphisms. Individuals who carry two *CYP3A5*3* alleles (*CYP3A5*3/*3*) have reduced or no expression of CYP3A5 compared with those homozygous for the wild-type *CYP3A5*1* allele (Hustert et al., 2001; Kuehl et al., 2001). We measured M1 formation by human liver microsomes isolated from individuals genotyped as *CYP3A5*1/*1* and individuals genotyped as *CYP3A5*3/*3* to determine the contribution of CYP3A5 to M1 formation in a system where CYP3A4 is present whereas CYP3A5 expression is absent or markedly reduced. In addition, these studies were used to probe the utility of M1 formation as a CYP3A5 phenotyping tool. After incubation with maraviroc (2 μM), the human liver microsomes isolated from donors homozygous for the *CYP3A5*3* alleles, exhibited a 79% decrease in formation of M1 compared with production by human liver microsomes isolated from donors homozygous for the *CYP3A5*1* allele ($P = 0.01$) (Fig. 3A). Furthermore, M1 was the most abundant metabolite formed using the *CYP3A5*1/*1* human liver microsomes (Fig. 3B). In human liver microsomes genotyped as *CYP3A5*3/*3*, M1, M2, and M3 all had comparable intensities (Fig. 3C).

M1 Is Formed via Hydroxylation of the Difluorocyclohexane Ring of Maraviroc. To determine the position of the P450-dependent monooxygenation that results in the formation of M1, mass spectrometry was performed using MS^2 and MS^3 scans after the UPLC separation of M1 from other maraviroc oxidative metabolites. These spectra were then compared with those for maraviroc as well as commercially available synthetic standards for 3-hydroxymethyl maraviroc, a metabolite with a hydroxyl group on the triazole moiety, and 4-hydroxyphenyl maraviroc, a metabolite with a hydroxyl group on the phenyl ring. Unlike those for 3-hydroxymethyl maraviroc, but similar to 4-hydroxyphenyl maraviroc, MS^2 scans of M1 resulted in two major product ions at *m/z* 296 and 405 (Fig. 4A), indicating that the hydroxyl group is not on the triazole moiety. This result was determined via comparison to a daughter ion *m/z* 280 of maraviroc that is a product of fragmentation with breakage at the tertiary amine

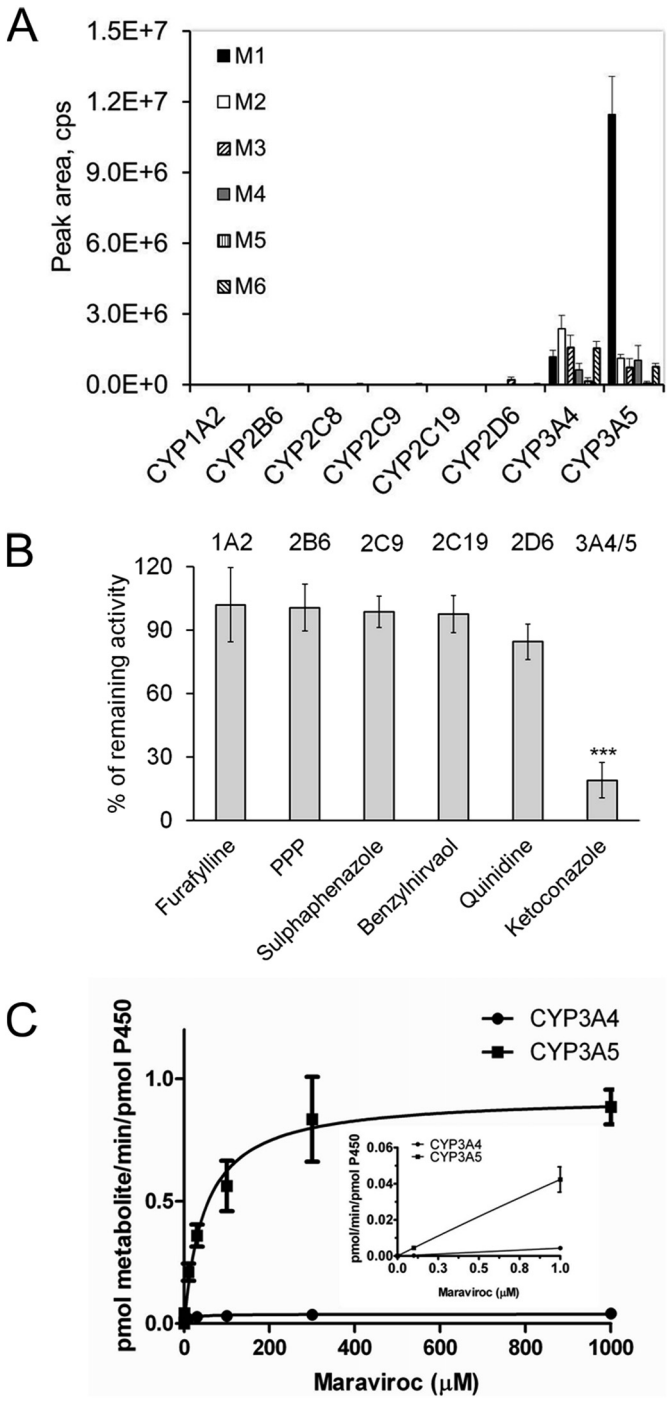

FIG. 2. CYP3A5 is the primary enzyme responsible for M1 formation. A, a panel of cDNA-expressed P450s was incubated with maraviroc followed by metabolite analysis. B, ketoconazole inhibited M1 formation. P450 chemical inhibitors were preincubated with human liver microsomes before the addition of maraviroc. The data are presented as percentage M1 formation activity remaining relative to vehicle control. The P450 targeted by the particular chemical inhibitor is shown at the top of the figure. ***, $P < 0.001$ compared with solvent control. C, M1 formation rate by CYP3A5 is greater than that by CYP3A4. cDNA-expressed CYP3A4 and CYP3A5 were incubated with 0.1 to 1000 μM maraviroc under initial rate conditions. M1 formation was determined using a maraviroc standard curve and maraviroc-d_6 as an internal standard. Kinetics data at maraviroc concentrations in the therapeutic range are shown in the inset. PPP, 2-phenyl-2-(1-piperidinyl) propane.

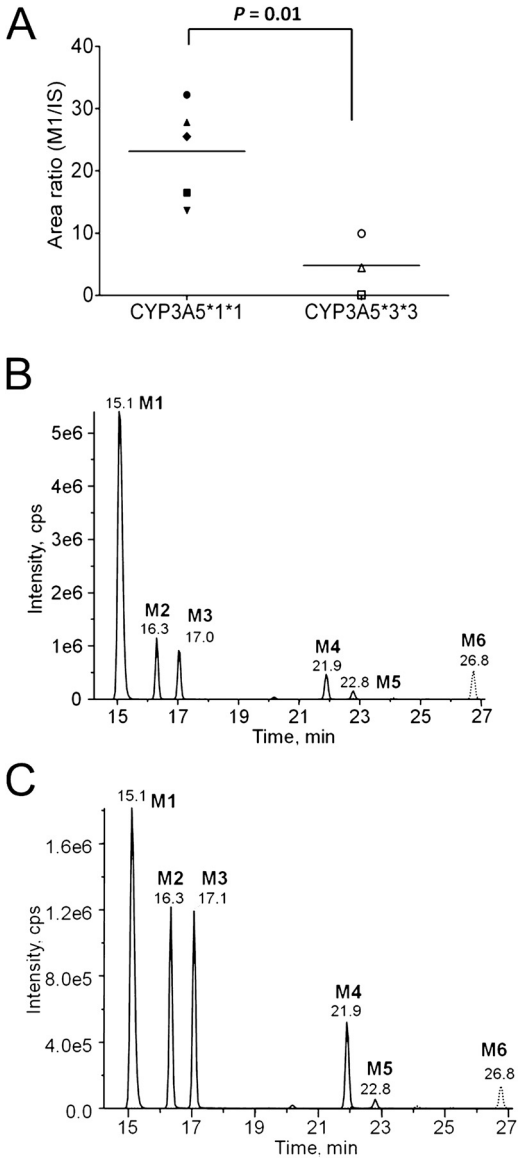

FIG. 3. M1 formation is decreased in human liver microsomes genotyped as *CYP3A5*3/*3*, and M1 is the major oxidative metabolite produced by *CYP3A5*1/*1* human liver microsomes. A, reduced M1 formation by human liver microsomes homozygous for a CYP3A5 nonfunctional allele. Human liver microsomes from individuals genotyped as *CYP3A5*1/*1* or *CYP3A5*3/*3* were incubated with 2 μM maraviroc and M1 formation was measured. Each data point represents the peak area ratio of M1 to maraviroc-d_6 (internal standard). The mean for each group is indicated by a horizontal line. B and C, representative chromatogram of oxidative metabolites from reactions of *CYP3A5*1/*1* human liver microsomes (B) and *CYP3A5*3/*3* human liver microsomes (C).

nitrogen of the tropane ring (Wright et al., 2010). This fragment then contains the difluorocyclohexane ring and phenyl ring of maraviroc but not the triazole moiety. Thus, we propose that the *m/z* 296 ion of M1 represents an oxygen (16 Da) insertion into this portion of the molecule, suggesting that the site of metabolism is either on the difluorocyclohexane ring or on the phenyl ring but not on the triazole moiety. To test this suggesting further, MS^3 scans were performed. Maraviroc daughter ion *m/z* 280 produced product ions at *m/z* 91, 106, and 117 (Fig. 4B). The ions with *m/z* 106 and 117 have been identified as phenyl ring-containing product ions of maraviroc (Shevchenko et al., 2009; Wright et al., 2010). In contrast, fragmentation of 4-hydroxyphenyl maraviroc daughter ion *m/z* 296 generated ions at *m/z* 122 and 133 (Fig. 4C), products resulting from one oxygen insertion on the phenyl ring-containing ions *m/z* 106 and 117, respectively. Unlike 4-hydroxyphenyl maraviroc but similar to maraviroc, fragmentation of M1 yielded phenyl ring-containing product ions at *m/z* 106 and 117 (Fig. 4D). From these data, it was concluded that M1 formation did not involve oxygenation of the phenyl ring. Therefore, because M1 formation did not appear to be involved in oxygen insertion on either the triazole ring or the phenyl ring of maraviroc, the oxygen insertion was assigned on the difluorocyclohexane ring (Fig. 4E), which matched other product ions (Fig. 4D). Fragmented ions with a loss of HF (20 Da) and $CH_2{=}CH_2$ (28 Da) from *m/z* 296 were found at 276 and 268, respectively. The loss of both HF and water (18 Da) from *m/z* 296 generated ions at *m/z* 258. A further loss of $CH_2{=}CH_2$ (28 Da) produced ions at *m/z* 230 (Fig. 4D). MS^2 and MS^3 scans were also used to confirm that M2 to M6 were indeed monooxygenated products as well and distinct from M1 (data not shown).

Mutation of Residues That Are Divergent between CYP3A4 and CYP3A5 Alters M1 Formation. Because studies have yet to be performed to identify the CYP3A5 residues that might confer substrate specificity, we leveraged our finding that M1 is formed preferentially by CYP3A5 over CYP3A4 and mutated several CYP3A5 residues predicted to be within SRSs based on alignment with CYP3A4. A number of residues outside of the predicted CYP3A5 SRSs were mutated to the corresponding amino acids of CYP3A4 as well to evaluate their contribution to the differential metabolism of maraviroc by these enzymes (Fig. 5). COS-7 cells were used as a model system for expression of CYP3A4 and CYP3A5 because they have been proven to express endogenous NADPH-cytochrome P450 reductase, which is necessary to support P450 enzyme-mediated metabolism (Guo et al., 2005). The untransfected cells did not exhibit activity toward maraviroc (data not shown). After transfection, protein expression of wild-type CYP3A5 and all mutants was measured using immunoblotting (Fig. 6, A and B). Similar to the maraviroc metabolism studies performed using human liver microsomes, the CYP3A-transfected COS-7 cells formed the oxidative metabolites of maraviroc with M1 to M3 being the most predominant. After protein normalization, a significant reduction in M1 formation by the L57F, S107P, L108F, G214D, L219F, L240V, I371M, S392V, T478L, and Q479G mutants was observed ($P < 0.02$) (Fig. 6C). Among them, G214D exhibited the greatest reduction of 88% compared with the wild-type CYP3A5. M1 formation by the L57F, L108F, and S107P mutants of CYP3A5 was decreased by 61, 59, and 72%, respectively. I224T mutation resulted in a loss of CYP3A5 expression, and thus no M1 was detected. We also found that mutations F146V, G186S, S206N, A296V, and V369I significantly increased M1 formation ($P < 0.05$). Mutations of F210L, S239C, and K243R did not significantly change the M1 formation activity of CYP3A5 ($P = 0.16$, 0.16, and 0.20, respectively). No obvious changes were detected for other mutations including F120L, K166T, K212R, V238I, T376V, R415L, and D477S (data not shown).

To gain a more comprehensive understanding of the effects of the mutations of CYP3A5 on catalytic activity, we also measured the formation of M2 and M3 in addition to that of M1. Wild-type CYP3A5 formed M1 at a higher level than M2 and M3 with metabolic ratios of M1/M2 and M1/M3 of 24.4 and 30.4, respectively (Table 1). In contrast, M1 formed by CYP3A4 was comparable to formation of M2 and M3 with M1/M2 and M1/M3 ratios of 1.5 and 1.6, respectively. Among the CYP3A5 mutants that were tested, L108F, G214D, and L57F resulted in a decrease in the M1/M2 ratio by 95, 75, and 52%, respectively, compared with wild-type CYP3A5. Furthermore, L108F, G214D, S107P, L57F, L240V, and I371M decreased the M1/M3 ratio by 95, 85, 64, 55, 51, and 51%, respectively. Thus, these mutations of CYP3A5 shifted formation of these metabolites

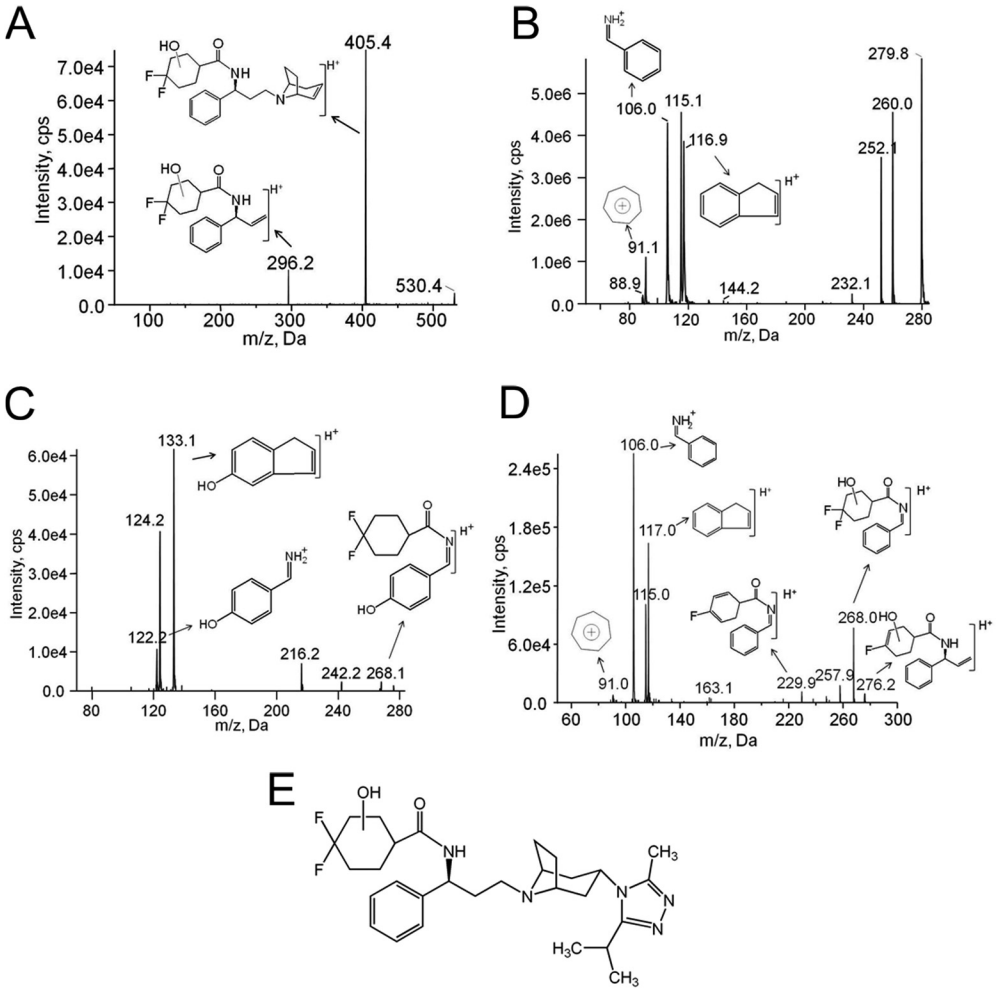

FIG. 4. M1 results from oxygen insertion on the difluorocyclohexane ring of maraviroc as determined by mass spectrometry. A, fragmentation profile of M1 with MS^2 scans of a precursor ion at *m/z* 530. MS^3 spectra of maraviroc (B), 4-hydroxyphenyl maraviroc (C), and M1 (D). E, the proposed structure of M1. MS^3 scans were performed using first/second precursor ions at *m/z* 514/280 for maraviroc and at *m/z* 530/296 for 4-hydroxyphenyl maraviroc and M1, respectively.

toward that of CYP3A4. In addition, F146V and L219F decreased the metabolic ratios of both M1/M2 and M1/M3; however, the differences from wild-type CYP3A5 were less than 50%. Unlike the other mutants, S206N increased M1/M2 and M1/M3 by 39 and 57%, respectively.

After the observation that mutation of certain CYP3A5 residues resulted in a metabolite profile similar to that of CYP3A4, we tested whether the reverse could occur if residues in CYP3A4 were mutated to the corresponding mismatched residues in CYP3A5. We analyzed CYP3A4 mutants including F57L, P107S, F108L, D214G, L479T,

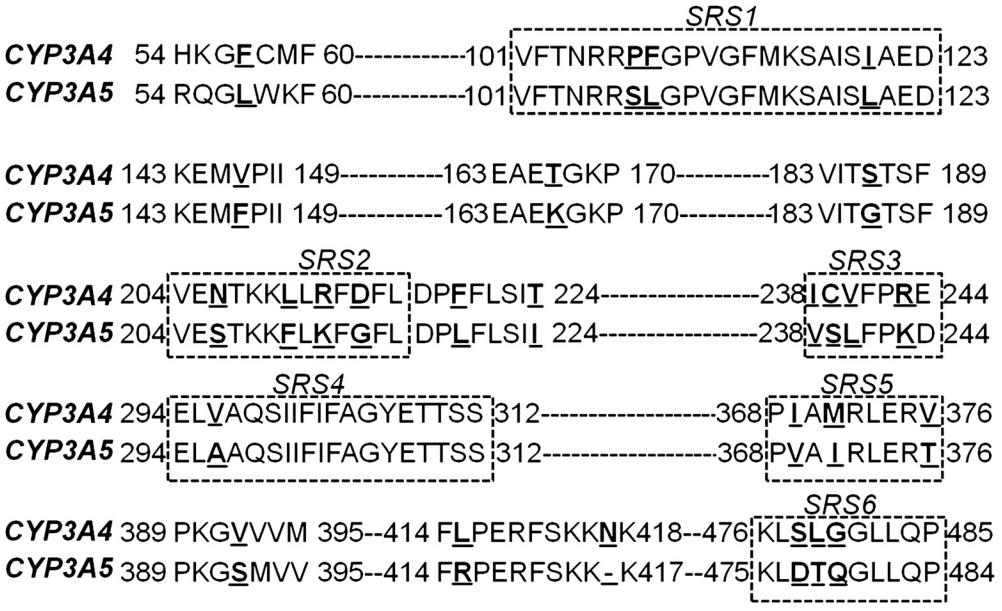

FIG. 5. Mutations of residues that are divergent between CYP3A4 and CYP3A5. The mismatched residues evaluated in this study are underlined and in bold font. The six previously reported putative substrate recognition sites SRS1 to SRS6 are shown in boxes (Emoto and Iwasaki, 2006).

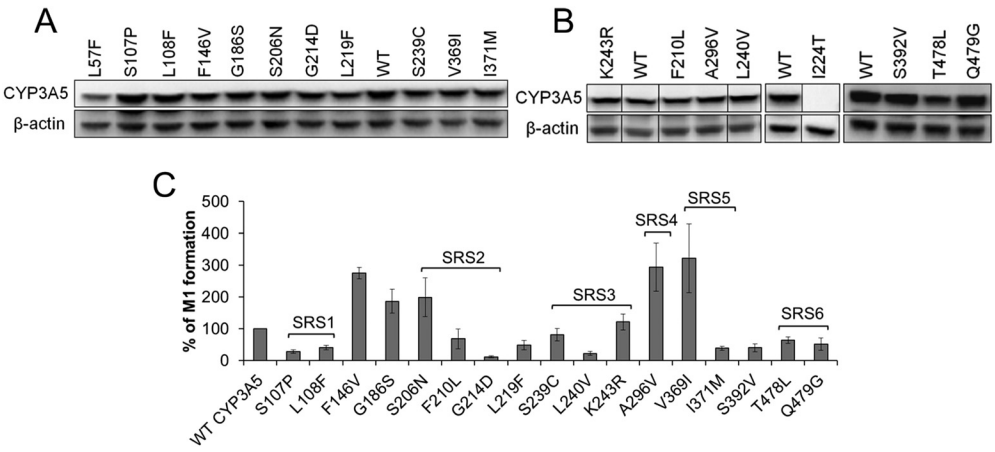

FIG. 6. Changes in M1 formation resulting from mutation of CYP3A5 toward CYP3A4 after normalization by protein expression. A and B, protein expression of CYP3A5 wild-type (WT) and mutants. C, M1 formation by CYP3A5 mutants relative to wild-type CYP3A5 after normalization to protein expression. Plasmids containing wild-type or mutant cDNA were transfected into COS-7 cells, and maraviroc was added to the medium 24 h after transfection. After 40 min of incubation, metabolites were measured in the medium, and protein expression was detected by immunoblot for normalization. SRS regions that the residues belong to are denoted on the graph. $P < 0.05$ for all mutants, except for F210L ($P = 0.16$), S239C ($P = 0.16$), and K243R ($P = 0.20$), compared with wild-type CYP3A5.

and deletion of N423 (ΔN423). CYP3A4 contains 503 amino acids, whereas CYP3A5 has 502 residues. N423 is the CYP3A4 amino acid that appears to be the additional amino acid, which is not present in CYP3A5 when the two sequences are aligned. Of interest, we found that although the L57F mutation of CYP3A5 shifted M1 formation toward CYP3A4 with a decrease of 61%, the reverse mutant of CYP3A4, F57L, had the opposite effect in that it increased M1 formation to 337% of that produced by wild-type CYP3A4 (Fig. 7). Other mutations including P107S, F108L, D214G, L479T, and ΔN423 did not have effects on M1 formation (data not shown).

Identification of Novel Dioxygenated Maraviroc Metabolites. Using the chromatographic method for maraviroc metabolite analysis that we developed, four previously unreported maraviroc dioxygenated metabolites (M7–M10) were identified in human liver microsome reactions by monitoring the transition *m/z* 546/312 (Fig. 8A). MS^2 fragmentation of the four metabolites all produced two major daughter ions at *m/z* 312 and 421, which have a 32-Da increase compared with the daughter ions of maraviroc *m/z* 280 and 389, respectively (Fig. 8B). This result suggested that the oxygen insertions were not on the triazole ring because neither of the fragment ions *m/z* 280 or *m/z* 389 contain the triazole ring. Further fragmentation of *m/z* 312 from M7 to M10 generated product ions *m/z* 106 and 117 (Fig. 8C), the two phenyl ring-containing ions found in the MS^3 spectra of maraviroc daughter ion *m/z* 280 (Fig. 4B), indicating that no oxygen insertions occurred on the phenyl ring of maraviroc. Therefore, the two hydroxyl groups were assigned to the difluorocyclohexane ring. The assignment was in agreement with other observed ions in the spectra, namely *m/z* 294 and 274, which are products of the *m/z* 312 daughter ion that are formed after the loss of a water molecule (18 Da) and a further loss of HF (20 Da), respectively (Fig. 8C). Consistent with the in vitro metabolism results using human liver microsomes, we found that the four dioxygenated metabolites were present in all the urine samples collected from the healthy volunteer (Fig. 8D). Similar to what was observed for the monooxygenated metabolites, CYP3A5 and CYP3A4 catalyzed the formation of all of the dioxygenated metabolites (data not shown).

Glucuronidation of Maraviroc. Glucuronidation has been proposed as a metabolic pathway for maraviroc in mice but not in humans (Walker et al., 2005); however, in the present study we have identified two maraviroc glucuronides that were detected using the transitions *m/z* 706/581 (M11, Fig. 9A) and *m/z* 706/389 (M12, Fig. 9A). MS^3 spectra of M11 with first/second precursor/product ions of 706/581 contained ions at *m/z* 472, 296, and 133 (Fig. 9B). The ion with *m/z*

TABLE 1

Comparison of metabolic ratios of CYP3A5 and its mutants with those of CYP3A4

The enzymes indicated were transiently expressed in COS-7 cells. Metabolism experiments for maraviroc were performed, and oxidative metabolites M1, M2, and M3 were measured as described under *Materials and Methods*. Metabolic ratios (M1/M2 and M1/M3) are presented as means ± S.D.

Name	M1/M2	M1/M3
CYP3A5	24.4 ± 1.3	30.4 ± 4.2
L57F	11.8 ± 1.2	13.6 ± 1.4
S107P	24.1 ± 2.7	10.9 ± 4.0
L108F	1.29 ± 0.05	1.7 ± 0.03
F146V	20.0 ± 2.9	25.6 ± 4.0
G186S	25.4 ± 1.5	38.9 ± 3.2
S206N	34.0 ± 2.1	47.6 ± 3.6
G214D	6.14 ± 0.2	4.6 ± 0.03
L219F	17.9 ± 0.4	16.7 ± 0.1
S239C	27.3 ± 4.0	42.3 ± 3.9
L240V	13.3 ± 6.3	14.9 ± 4.9
V369I	18.2 ± 4.5	25.1 ± 2.8
I371M	20.3 ± 2.8	15.0 ± 1.5
S392V	22.5 ± 0.1	18.8 ± 2.3
T478L	25.6 ± 2.7	38.1 ± 2.7
Q479G	25.6 ± 2.2	23.4 ± 1.1
CYP3A4	1.5 ± 0.5	1.6 ± 0.8

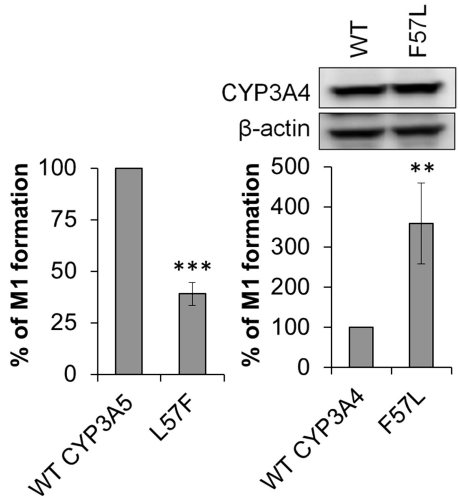

FIG. 7. Residue 57 contributes to the differential formation of M1 by CYP3A4 and CYP3A5. Decreased M1 formation by the CYP3A5 L57F mutant and increased M1 formation by the CYP3A4 F57L mutant relative to that by wild-type CYP3A5 and CYP3A4, respectively. Protein expression of wild-type (WT) CYP3A4 and the F57L mutant is shown above the right panel and expression of CYP3A5 L57F is shown in Fig. 6A. Metabolite formation was normalized to protein expression as measured using immunoblotting. **, $P < 0.01$; ***, $P < 0.001$, compared with wild-type.

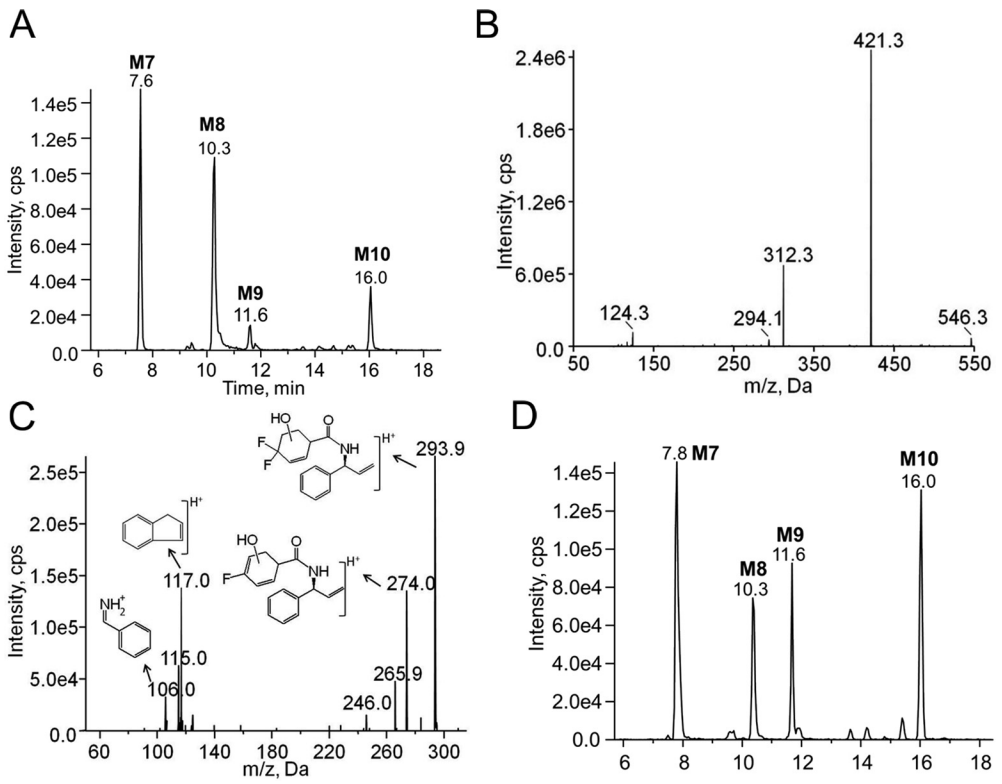

FIG. 8. Chromatograms and MS^n spectra of the maraviroc dioxygenated metabolites. A, chromatogram of dioxygenated maraviroc metabolites (M7–M10) detected using the transition *m/z* 546 → 312 from metabolism reactions using human liver microsomes. B, representative MS^2 spectra of M7 to M10 with the precursor ion *m/z* 546. C, representative MS^3 spectra of M7 to M10 with first/second precursor ions at *m/z* 546/312. The proposed structures of fragmented ions are shown near the corresponding peaks. D, chromatogram of dioxygenated maraviroc metabolites (M7–M10) detected in urine collected at 0 to 2 h from a healthy volunteer using the transition *m/z* 546 → 312.

472 is a product resulting from a glucuronic acid (176 Da) conjugation on the ion with *m/z* 296, an ion with one oxygen insertion compared with maraviroc daughter ion *m/z* 280. The ion with *m/z* 133 has the same mass as a product ion (*m/z* 133) of 4-hydroxyphenyl-maraviroc (Fig. 4C). Therefore, the conjugation of glucuronic acid was assigned to the phenyl ring. Unlike M11, fragmentation of M12 generated two major ions, *m/z* 389 and *m/z* 280, the same two daughter ions produced via fragmentation of maraviroc (Fig. 9C). MS^3 spectra confirmed that these two ions were indeed the same in both maraviroc and M12, suggesting that the glucuronidation occurred on the triazole

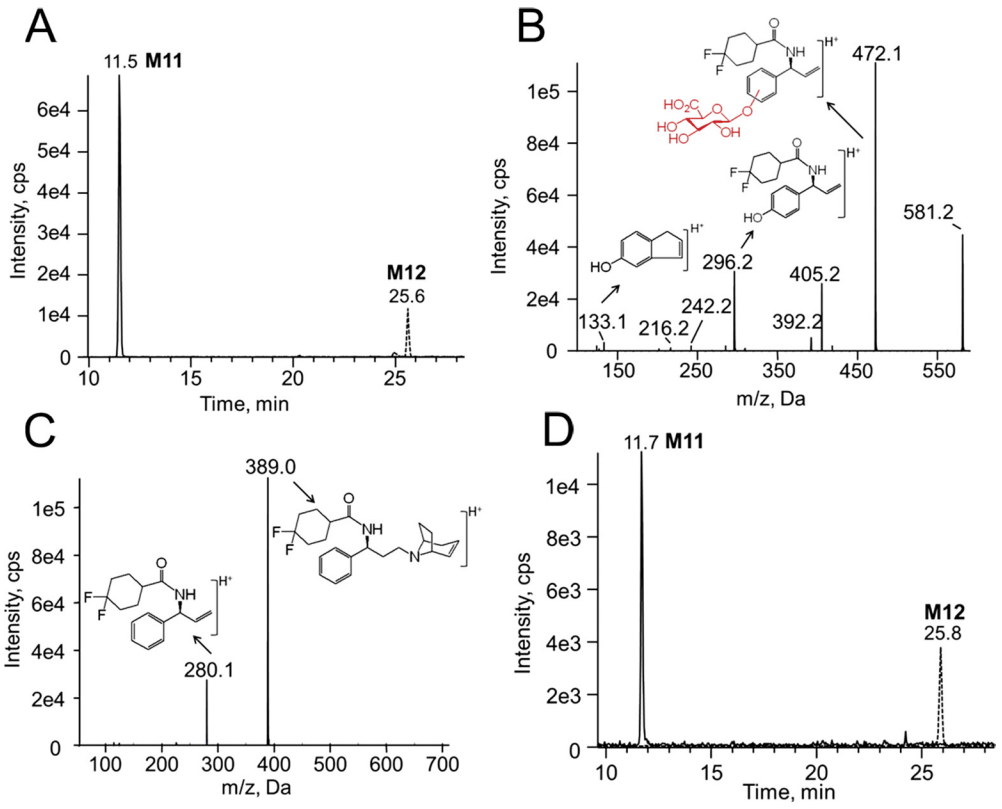

FIG. 9. Chromatograms and MS^n spectra of maraviroc glucuronides. A, multiple reaction monitoring chromatogram of maraviroc glucuronides with transitions at *m/z* 706 → 581 (M11) and at *m/z* 706 → 389 (M12) from metabolism reactions using human liver microsomes. B, MS^3 spectra of M11 monitoring first/second precursor ions at *m/z* 706/581. C, MS^2 spectra of M12 monitoring precursor ion at *m/z* 706. The proposed structures of fragmented ions are shown near the corresponding peaks. D, multiple reaction monitoring chromatogram of maraviroc glucuronides with transition at *m/z* 706 → 581 (M11) and at *m/z* 706 → 389 (M12) in urine collected at 0 to 2 h from the volunteer.

moiety after oxidation. Consistently, we also found that the two glucuronides were present in the human urine samples (Fig. 9D).

Discussion

In this study, a novel chromatographic method was developed for the separation and quantitation of oxidative metabolites and glucuronides of maraviroc. We found six major monooxygenated metabolites (M1-M6), four novel dioxygenated metabolites (M7-M10), and two previously unidentified glucuronides (M11 and M12) using human liver microsomes and confirmed that the metabolite profile was similar in plasma and/or urine samples after administration of maraviroc to a healthy volunteer. The separation method that we developed has utility in future studies of maraviroc metabolism in both basic and clinical research. Furthermore, because maraviroc is currently used clinically to treat HIV and is being investigated for additional use in HIV prevention, the data presented here are valuable in that we provide the first detailed information regarding the biotransformation of maraviroc both in vitro and in vivo.

We identified CYP3A4 and CYP3A5 as the major P450s involved in maraviroc oxidation, which will be helpful in understanding drug-drug interactions of maraviroc with other drugs. It is known that maraviroc plasma concentration and exposure are significantly changed when coadministered with CYP3A inducers or inhibitors (Abel et al., 2008b; Boffito and Abel, 2008). The M1 formation activity of CYP3A5 exhibited an evident difference from that of CYP3A4. This was further confirmed by the observation that there was a marked reduction in M1 formation by human liver microsomes genotyped as the homozygous *CYP3A5*3* allele that do not express CYP3A5. In addition, N-dealkylation and oxidation have been reported to be the two major pathways responsible for the metabolism-dependent clearance of maraviroc (Abel et al., 2008a). Previous studies reported a K_m of 21 μM and V_{max} of 0.45 pmol $\cdot$ min^{-1} $\cdot$ pmol P450^{-1} for N-dealkylation of maraviroc using human liver microsomes and a K_m of 13 μM and V_{max} of 3 pmol $\cdot$ min^{-1} $\cdot$ pmol P450^{-1} for the formation of this same metabolite using cDNA-expressed CYP3A4 (Hyland et al., 2008); here we demonstrated that CYP3A5 plays a primary role in the formation of M1 with K_m of 48.9 μM and V_{max} of 0.93 pmol $\cdot$ min^{-1} $\cdot$ pmol P450^{-1}. We also detected the N-dealkylated metabolite of maraviroc in both plasma and urine samples. The peak area ratio of the N-dealkylated metabolite to M1 in plasma varied from 0.3 to 2.6 with time over a period of 24 h after the dose, suggesting that monooxygenation of maraviroc may not be a minor pathway of maraviroc metabolism compared with the N-dealkylation. This result indicates that in addition to N-dealkylation, monooxygenation should also be monitored to gain a more complete understanding of the mechanism(s) of maraviroc clearance. Taken together, our results indicate that M1 formation is primarily mediated by CYP3A5, and, thus, maraviroc is potentially useful as a probe substrate for CYP3A5. The use of maraviroc as a CYP3A5 probe substrate can be applied to in vitro drug-drug interaction studies to identify potential inducers or inhibitors of CYP3A5 in the process of drug development.

In addition, several aspects of maraviroc make it an attractive candidate for potential consideration as a CYP3A5 clinical phenotyping probe: 1) it is a U.S. Food and Drug Administration-approved oral drug; 2) maraviroc has an excellent clinical safety profile (Hardy et al., 2010); and 3) M1 was detected as one of the major oxidative metabolites in urine as early as 0 to 2 h after maraviroc administration (data not shown), possibly making maraviroc a noninvasive phenotyping probe through analysis of urine samples. Several studies have shown that CYP3A5 is involved in metabolism of drugs including vincristine (Dennison et al., 2006, 2007, 2008), tacrolimus (Kamdem et al., 2005; Renders et al., 2007), and cyclosporine (Min et al., 2004); however, these drugs all have demonstrated toxicities (Levitt and Prager, 1975; Bennett and Norman, 1986; Naesens et al., 2009; Guilhaumou et al., 2011).

We found a single residue, 57, that when mutated in CYP3A5 (L to F) shifted the CYP3A5-dependent M1 formation to mirror that of CYP3A4 and vice versa (CYP3A4 F to L). This is the first time that a residue that confers a switch in the activity between CYP3A4 and CYP3A5 has been identified. Our study provided the first experimental evidence, to the best of our knowledge, for the importance of this residue for CYP3A activity as well as its role in differentiating activities between CYP3A4 and CYP3A5. A recent crystal structure has shown that the CYP3A4 residue F57 is involved in the binding of the CYP3A4 substrate ritonavir (Sevrioukova and Poulos, 2010).

Several studies have suggested an important role for SRS1 residue F108, which resides in the Phe cluster (Phe108, Phe213, Phe215, Phe219, Phe220, Phe241, and Phe304) that forms a hydrophobic roof for the CYP3A4 active site, in CYP3A4 catalytic activity(Williams et al., 2004; Yano et al., 2004). Replacement of Phe108 in CYP3A4 to the corresponding CYP3A5 residue L decreased metabolism of testosterone and aflatoxin B1 (Wang et al., 1998). The CYP3A4-ritonavir crystal structure showed that Phe108 formed a hydrophobic pocket for ritonavir binding along with several other residues (Sevrioukova and Poulos, 2010). In addition, computational modeling predicted that Phe108 in CYP3A4 is involved in maraviroc binding via van der Waals interaction (Mannu et al., 2011). A previous CYP3A5 homology model constructed on the basis of the CYP3A4 crystal structure showed that the overall folding of CYP3A5 overlaid with the folds of CYP3A4 (Pearson et al., 2007), suggesting that Leu108 might be located in the roof of the CYP3A5 active site as it is in CYP3A4. Our current study showed that mutation L108F in CYP3A5 reduced M1 formation, confirming its importance to CYP3A5 activity. In addition, the formation of M2 and M3 was increased compared with that of wild-type CYP3A5. The resultant metabolite profile resembles that of CYP3A4 with similar metabolic ratios. Similar to residue Phe108, residue Phe219 in the hydrophobic pocket of CYP3A4 is replaced by L in CYP3A5. After mutation of L to F at 219 in CYP3A5, we also observed a reduction in M1 formation. The increased size in the side chain for the mutation L to F at 108 and 219 may strengthen the effects of the characteristic "Phe cluster," thereby making the shape of the CYP3A5 substrate binding pocket more like that of CYP3A4, resulting in the change of CYP3A5 activity toward that of CYP3A4.

Mutation of CYP3A5 SRS2 residue Gly214 to CYP3A4 residue Asp214, a residue located between the hydrophobic residues Phe213 and Phe215, resulted in a pronounced effect with 88% reduction of CYP3A5 activity for M1 formation. CYP3A4 SRS3 residue Val240 belongs to this hydrophobic ceiling of the active site along with the Phe cluster and was shown to contribute to progesterone binding (Williams et al., 2004). The mutation of CYP3A5 L240V also resulted in a marked decrease in M1 formation. These data underscore the importance of the hydrophobic roof in the active site, which might play a role in CYP3A4 and CYP3A5 substrate specificity.

In summary, we found that CYP3A4 and CYP3A5 were the major enzymes responsible for maraviroc oxidation and that CYP3A5 was the primary enzyme responsible for the formation of a major monooxygenated metabolite of maraviroc, we determined that the divergent residue 57 within CYP3A4 and CYP3A5 contributed to their differential activities toward maraviroc, and we also identified novel secondary deoxygenated and glucuronidated metabolites of maraviroc. Taken together, these studies suggest that maraviroc may have use as a probe substrate for CYP3A5, besides filling the gap in understanding of maraviroc metabolism. In addition, the present study

has provided novel biochemical information regarding the contribution of divergent residues to the activity of both CYP3A4 and CYP3A5.

Acknowledgments

We kindly acknowledge Drs. Walter C. Hubbard and Teresa L. Parsons (Johns Hopkins University School of Medicine) for helpful suggestions during development of chromatography. We are grateful to Dr. Jin Zhang (Johns Hopkins University School of Medicine) for providing COS-7 cells.

Authorship Contributions

Participated in research design: Lu, Hendrix, and Bumpus.

Conducted experiments: Lu.

Performed data analysis: Lu and Bumpus.

Wrote or contributed to the writing of the manuscript: Lu, Hendrix, and Bumpus.

References

Abel S, Russell D, Whitlock LA, Ridgway CE, Nedderman AN, and Walker DK (2008a) Assessment of the absorption, metabolism and absolute bioavailability of maraviroc in healthy male subjects. *Br J Clin Pharmacol* **65 (Suppl):**60–67.

Abel S, van der Ryst E, Rosario MC, Ridgway CE, Medhurst CG, Taylor-Worth RJ, and Muirhead GJ (2008b) Assessment of the pharmacokinetics, safety and tolerability of maraviroc, a novel CCR5 antagonist, in healthy volunteers. *Br J Clin Pharmacol* **65 (Suppl):**5–18.

Bennett WM and Norman DJ (1986) Action and toxicity of cyclosporine. *Annu Rev Med* **37:**215–224.

Boffito M and Abel S (2008) A review of the clinical pharmacology of maraviroc. Introduction. *Br J Clin Pharmacol* **65 (Suppl):**1–4.

Daly AK (2006) Significance of the minor cytochrome P450 3A isoforms. *Clin Pharmacokinet* **45:**13–31.

Dennison JB, Jones DR, Renbarger JL, and Hall SD (2007) Effect of CYP3A5 expression on vincristine metabolism with human liver microsomes. *J Pharmacol Exp Ther* **321:**553–563.

Dennison JB, Kulanthaivel P, Barbuch RJ, Renbarger JL, Ehlhardt WJ, and Hall SD (2006) Selective metabolism of vincristine in vitro by CYP3A5. *Drug Metab Dispos* **34:**1317–1327.

Dennison JB, Mohutsky MA, Barbuch RJ, Wrighton SA, and Hall SD (2008) Apparent high CYP3A5 expression is required for significant metabolism of vincristine by human cryopreserved hepatocytes. *J Pharmacol Exp Ther* **327:**248–257.

Domanski TL, Liu J, Harlow GR, and Halpert JR (1998) Analysis of four residues within substrate recognition site 4 of human cytochrome P450 3A4: role in steroid hydroxylase activity and α-naphthoflavone stimulation. *Arch Biochem Biophys* **350:**223–232.

Dorr P, Westby M, Dobbs S, Griffin P, Irvine B, Macartney M, Mori J, Rickett G, Smith-Burchnell C, Napier C, et al. (2005) Maraviroc (UK-427,857), a potent, orally bioavailable, and selective small-molecule inhibitor of chemokine receptor CCR5 with broad-spectrum anti-human immunodeficiency virus type 1 activity. *Antimicrob Agents Chemother* **49:**4721–4732.

Egbelakin A, Ferguson MJ, MacGill EA, Lehmann AS, Topletz AR, Quinney SK, Li L, McCammack KC, Hall SD, and Renbarger JL (2011) Increased risk of vincristine neurotoxicity associated with low CYP3A5 expression genotype in children with acute lymphoblastic leukemia. *Pediatr Blood Cancer* **56:**361–367.

Emoto C and Iwasaki K (2006) Enzymatic characteristics of CYP3A5 and CYP3A4: a comparison of in vitro kinetic and drug-drug interaction patterns. *Xenobiotica* **36:**219–233.

Fätkenheuer G, Pozniak AL, Johnson MA, Plettenberg A, Staszewski S, Hoepelman AI, Saag MS, Goebel FD, Rockstroh JK, Dezube BJ, et al. (2005) Efficacy of short-term monotherapy with maraviroc, a new CCR5 antagonist, in patients infected with HIV-1. *Nat Med* **11:**1170–1172.

Guilhaumou R, Solas C, Bourgarel-Rey V, Quaranta S, Rome A, Simon N, Lacarelle B, and Andre N (2011) Impact of plasma and intracellular exposure and CYP3A4, CYP3A5, and ABCB1 genetic polymorphisms on vincristine-induced neurotoxicity. *Cancer Chemother Pharmacol* **68:**1633–1638.

Guo Y, Zhang Y, Wang Y, Chen X, Si D, Zhong D, Fawcett JP, and Zhou H (2005) Role of CYP2C9 and its variants (CYP2C9*3 and CYP2C9*13) in the metabolism of lornoxicam in humans. *Drug Metab Dispos* **33:**749–753.

Hardy WD, Gulick RM, Mayer H, Fätkenheuer G, Nelson M, Heera J, Rajicic N, and Goodrich J (2010) Two-year safety and virologic efficacy of maraviroc in treatment-experienced patients with CCR5-tropic HIV-1 infection: 96-week combined analysis of MOTIVATE 1 and 2. *J Acquir Immune Defic Syndr* **55:**558–564.

Harlow GR and Halpert JR (1997) Alanine-scanning mutagenesis of a putative substrate recognition site in human cytochrome P450 3A4. Role of residues 210 and 211 in flavonoid activation and substrate specificity. *J Biol Chem* **272:**5396–5402.

He YA, He YQ, Szklarz GD, and Halpert JR (1997) Identification of three key residues in substrate recognition site 5 of human cytochrome P450 3A4 by cassette and site-directed mutagenesis. *Biochemistry* **36:**8831–8839.

Hooper DK, Fukuda T, Gardiner R, Logan B, Roy-Chaudhury A, Kirby CL, Vinks AA, and Goebel J (2012) Risk of tacrolimus toxicity in CYP3A5 nonexpressors treated with intravenous nicardipine after kidney transplantation. *Transplantation* **93:**806–812.

Hustert E, Haberl M, Burk O, Wolbold R, He YQ, Klein K, Nuessler AC, Neuhaus P, Klattig J, Eiselt R, et al. (2001) The genetic determinants of the CYP3A5 polymorphism. *Pharmacogenetics* **11:**773–779.

Hyland R, Dickins M, Collins C, Jones H, and Jones B (2008) Maraviroc: in vitro assessment of drug-drug interaction potential. *Br J Clin Pharmacol* **66:**498–507.

Kamdem LK, Streit F, Zanger UM, Brockmöller J, Oellerich M, Armstrong VW, and Wojnowski L (2005) Contribution of CYP3A5 to the in vitro hepatic clearance of tacrolimus. *Clin Chem* **51:**1374–1381.

Khan KK and Halpert JR (2000) Structure-function analysis of human cytochrome P450 3A4 using 7-alkoxycoumarins as active-site probes. *Arch Biochem Biophys* **373:**335–345.

Khan KK, He YQ, Domanski TL, and Halpert JR (2002) Midazolam oxidation by cytochrome P450 3A4 and active-site mutants: an evaluation of multiple binding sites and of the metabolic pathway that leads to enzyme inactivation. *Mol Pharmacol* **61:**495–506.

Kuehl P, Zhang J, Lin Y, Lamba J, Assem M, Schuetz J, Watkins PB, Daly A, Wrighton SA, Hall SD, et al. (2001) Sequence diversity in CYP3A promoters and characterization of the genetic basis of polymorphic CYP3A5 expression. *Nat Genet* **27:**383–391.

Levitt LP and Prager D (1975) Mononeuropathy due to vincristine toxicity. *Neurology* **25:**894–895.

Mannu J, Jenardhanan P, and Mathur PP (2011) A computational study of CYP3A4 mediated drug interaction profiles for anti-HIV drugs. *J Mol Model* **17:**1847–1854.

Min DI, Ellingrod VL, Marsh S, and McLeod H (2004) CYP3A5 polymorphism and the ethnic differences in cyclosporine pharmacokinetics in healthy subjects. *Ther Drug Monit* **26:**524–528.

Naesens M, Kuypers DR, and Sarwal M (2009) Calcineurin inhibitor nephrotoxicity. *Clin J Am Soc Nephrol* **4:**481–508.

Pearson JT, Wahlstrom JL, Dickmann LJ, Kumar S, Halpert JR, Wienkers LC, Foti RS, and Rock DA (2007) Differential time-dependent inactivation of P450 3A4 and P450 3A5 by raloxifene: a key role for C239 in quenching reactive intermediates. *Chem Res Toxicol* **20:**1778–1786.

Renders L, Frisman M, Ufer M, Mosyagin I, Haenisch S, Ott U, Caliebe A, Dechant M, Braun F, Kunzendorf U, et al. (2007) CYP3A5 genotype markedly influences the pharmacokinetics of tacrolimus and sirolimus in kidney transplant recipients. *Clin Pharmacol Ther* **81:**228–234.

Rendic S and Di Carlo FJ (1997) Human cytochrome P450 enzymes: a status report summarizing their reactions, substrates, inducers, and inhibitors. *Drug Metab Rev* **29:**413–580.

Roussel F, Khan KK, and Halpert JR (2000) The importance of SRS-1 residues in catalytic specificity of human cytochrome P450 3A4. *Arch Biochem Biophys* **374:**269–278.

Sevrioukova IF and Poulos TL (2010) Structure and mechanism of the complex between cytochrome P4503A4 and ritonavir. *Proc Natl Acad Sci USA* **107:**18422–18427.

Shevchenko VP, Nagaev IY, and Myasoedov NF (2009) Introduction of hydrogen isotopes into maraviroc and mass-spectrometric study of deuterium distribution. *Radiochemistry* **51:**175–177.

Takashina Y, Naito T, Mino Y, Yagi T, Ohnishi K and Kawakami J (2012) Impact of CYP3A5 and ABCB1 gene polymorphisms on fentanyl pharmacokinetics and clinical responses in cancer patients undergoing conversion to a transdermal system. *Drug Metab Pharmacokinet* http://dx.doi.org/10.2133/dmpk.DMPK-11-RG-134.

van Schaik RH, van der Heiden IP, van den Anker JN, and Lindemans J (2002) CYP3A5 variant allele frequencies in Dutch Caucasians. *Clin Chem* **48:**1668–1671.

Walker DK, Abel S, Comby P, Muirhead GJ, Nedderman AN, and Smith DA (2005) Species differences in the disposition of the CCR5 antagonist, UK-427,857, a new potential treatment for HIV. *Drug Metab Dispos* **33:**587–595.

Wang H, Dick R, Yin H, Licad-Coles E, Kroetz DL, Szklarz G, Harlow G, Halpert JR, and Correia MA (1998) Structure-function relationships of human liver cytochromes P450 3A: aflatoxin B1 metabolism as a probe. *Biochemistry* **37:**12536–12545.

Williams PA, Cosme J, Vinkovic DM, Ward A, Angove HC, Day PJ, Vonrhein C, Tickle IJ, and Jhoti H (2004) Crystal structures of human cytochrome P450 3A4 bound to metyrapone and progesterone. *Science* **305:**683–686.

Wright P, Alex A, Nyaruwata T, Parsons T, and Pullen F (2010) Using density functional theory to rationalise the mass spectral fragmentation of maraviroc and its metabolites. *Rapid Commun Mass Spectrom* **24:**1025–1031.

Yano JK, Wester MR, Schoch GA, Griffin KJ, Stout CD, and Johnson EF (2004) The structure of human microsomal cytochrome P450 3A4 determined by X-ray crystallography to 2.05-A resolution. *J Biol Chem* **279:**38091–38094.

Zawaira A, Ching LY, Coulson L, Blackburn J, and Wei YC (2011) An expanded, unified substrate recognition site map for mammalian cytochrome P450s: analysis of molecular interactions between 15 mammalian CYP450 isoforms and 868 substrates. *Curr Drug Metab* **12:**684–700.

Address correspondence to: Dr. Namandjé N. Bumpus, Department of Pharmacology and Molecular Sciences, The Johns Hopkins University School of Medicine, 725 N. Wolfe St., WBSB 302, Baltimore, MD 21205. E-mail: nbumpus1@jhmi.edu